Performance Predictions of RF Heated Plasma in EAST

S. Ding 1), B. Wan 1), X. Zhang 1), R. V. Budny 2), Y. Guo 1), D. McCune 2), P. Xu 1), J. Yang 1), J. Qian 1), Y. Shi 1), F. Wang 1), S. M. Kaye 2)

1) Institute of Plasma Physics, Chinese Academy of Sciences, Hefei, Anhui, 230031, China
2) PPPL, Princeton University, P.O. Box 451, Princeton, NJ 08543, USA

E-mail contact of main author: archangel@ipp.ac.cn

Abstract. The scenario development of high power L- and H-mode plasma in EAST tokamak with current parameters is reported in this article. The simulation firstly uses PTRANSP in combination with TSC to explore the feature of EAST plasma with various RF auxiliary heating methods, including ICRH and LHCD system. GLF23 transport model was found to be the best fit of experiment data in comparison with MMM95 and MMM08 models. A series of ICRH scanning simulation is performed to optimize parameters of new ICRH system in EAST. Within the current auxiliary power limits, the highest plasma stored energy that can be achieved as well as other related plasma parameters are predicted. Possible discharge length of high power plasma can be 8-200 s, depending on the volt-second consumption in different scenarios. Various phenomena are also reported, including the influence of different fraction of RF power on their deposition behavior, as well as on thermal diffusivity. The scenario development provides the capability of current EAST machine. This study will be compared with experiments in EAST to validate existing theoretical transport models in PTRANSP.

1. Introduction

After several successful campaigns of experiment and continual upgrade of its internal structure as well as the radio frequency (RF) auxiliary heating system [1], Experimental Advanced Superconducting Tokamak (EAST) has the potential to achieve high power L mode even H mode within the limit of current parameters. The issue of high power simulation, including L mode and H mode boundary for EAST plasma is presented in this article. This study for the first time uses PTRANSP code [2, 3], in combination with TSC code [4] (for the initial parameters and the fixed boundary) to generate self-consistent time-dependent integrated predictions for EAST plasma. It is necessary for this set of simulations to provide basic insight into the possibility of achieving H mode and the feature of high power plasma for EAST scenario development with current parameters.

In section 2, target plasma studied in PTRANSP is discussed as well as the modeling details. Results of ICRH simulation will be shown in section 3. With the optimized ICRF parameters, high power EAST simulation is carried out and the results are then given in section 4. Conclusion of this article is presented in section 5.

2. Target Plasma and Modeling Details

A reference shot (shot# 12755) was selected from EAST spring campaign in 2009. Since there is no density profile data so far, presumed profile of L mode boundary (FIG. 1), which roughly fits the three channels of line-averaged density measurements (shot# 12755) along different chords, is used both in TSC and PTRANSP runs. Here, ρ is a magnetic flux coordinate as the square root of the normalized toroidal flux. H mode discharge is not yet

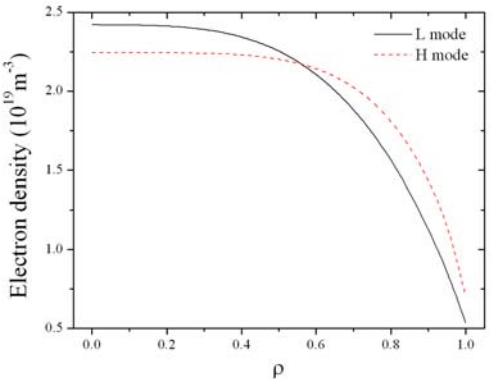

FIG. 1. Density profiles for L (solid line) and H (dash line) mode boundary used in this study. The profile of L mode fits EAST experiment data (shot# 12755), while the H mode profile is inferred from the reports of other tokamaks. The line-averaged values in this figure are both 2.0×10^{19} m^{-3}.

achieved in EAST. In FIG. 1, the H mode boundary density profile is assumed, which is inferred from the reports of other tokamaks [5]. Several theoretical transport models had been tested in PTRANSP runs, while X-ray Crystal Spectrometer (XCS) gave electron and ion temperature profiles and electron temperature experiment data was also provided by Soft X-ray Pulse Height Analysis (SXPHA) (FIG. 2(a)). Further, three Ohmic shots with different line-averaged density were also simulated as benchmark against experiment data (FIG. 2(b)). Instinct rotation and rotation driven by RF heating, which are not included in current theoretical transport models, comprise the plasma rotation in current EAST. So the predictive ion temperature in this study can perhaps be some percents lower than the results with actual rotation in EAST plasma driven by RF power, due to the E×B shear on turbulence suppression. Nevertheless, the stiff GLF23 model [6,7] (with Chang-Hinton model in plasma core region) fits the experiment data best in comparison with MMM95 [8] and MMM08 [9] models. GLF23 model was chosen for high power EAST simulation in this study.

In this study, the plasmas of 500 kA plasma current and double null configuration were studied. The toroidal field was usually set to 2 T@175 cm and can be scaled down to 1.8 T or up to 2.56 T in some runs for comparison. According to PEDESTAL module [10], the LH transition power varies from 1.0 to 1.8 MW depending on the line-averaged density, which was varied from 1.5 to 3.0×10^{19} m^{-3}, and the toroidal field. Two ICRF heating regimes were studied, including ^{3}He minority heating (MH) and H second harmonic heating (SH) in D plasma. The concentration of H (n_H/n_e) was set to 20%, considering the reality of EAST wall conditioning, which has high hydrogen retention and high wall recycling. Carbon is considered as the primary impurity. Due to transfer and coupling loss, the possible maximum effective auxiliary powers for current EAST parameters are $P_{ICRF}\leq1.4$ MW, $P_{LHW}\leq1.0$ MW. The predicted radiated power in PTRANSP is far below the realistic level. Lacking of radiation data for EAST experiment, the fraction of radiated power was assumed to be from 30% to 50% of total injected power in this work. Therefore, the assumed maximum effective auxiliary power used in PTRANSP runs was set to 1.7 MW. In PTRANSP runs, the TORIC full wave code [11] is used to model ICRF heating process. In this article, poloidal modes are 63, thus, the number of poloidal mesh points is 128. Besides, the number of radial mesh points is 323. Symmetric $n_{//}$ spectra of $n_{//}$=23 is used with the real antenna geometry in EAST. The effect of 2.45 GHz LHCD can be simulated by LSC code [12] in PTRANSP. The phasing of LH coupler is 0° in this study.

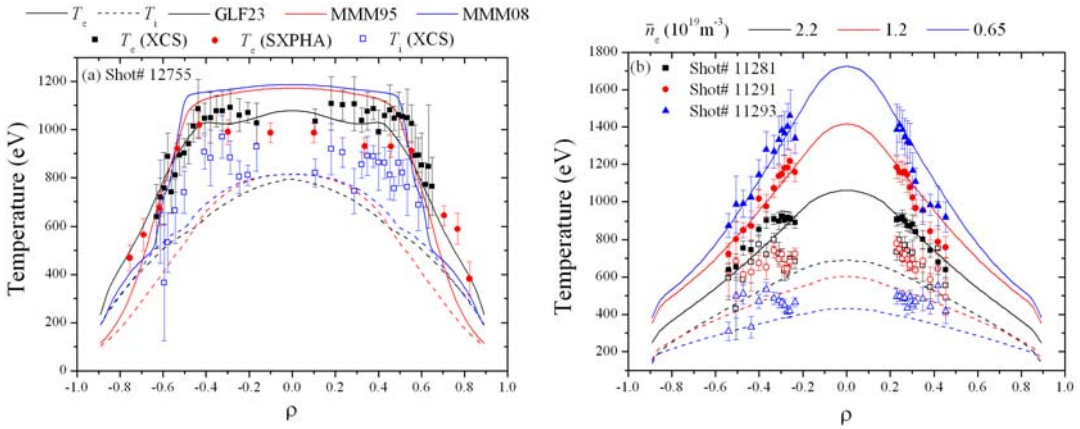

FIG. 2. (a) Comparison of calculated temperature profile by different theoretical models (lines in different colors, and solid lines for electron temperature, dash lines for ion temperature) and experiment data (solid dots for electron temperature and open dots for ion temperature). (b) TRANSP fits (lines) and experiment data (dots) of Ohmic shots with different line-averaged densities (in different colors) using GLF23 in combination with Chang-Hinton model. The meaning of other symbols is the same as (a).

3. ICRH simulation

It is well known that ICRF minority heating using ^{3}He in D plasma has high absorption efficiency in thermal ion heating in comparison with other ICRH regimes used in tokamak. ICRH would play critical role in EAST experiment not only in the future but also at present. Now, it is capable to conduct ^{3}He minority heating in EAST. Optimizing ICRH parameters is also necessary for further EAST high power simulation. In this simulation, some features of ^{3}He minority heating plasma are summarized with real EAST parameters. It is designed on a low level of ICRF power (400 kW) and medium density (2.0×10^{19} m^{-3}, mostly), using the L mode density profile in FIG. 1, to find out the dependence of ICRF power deposition feature on various plasma parameters. The frequency range of current ICRF system is 25-70 MHz. 25 MHz is used for ^{3}He minority heating in this simulation. During each scanning, plasma equilibrium and configuration change little.

FIG. 3 shows the results of B_T scanning in ICRF ^{3}He minority heating plasma with constant ^{3}He concentration of 3%. The ICRF power is kept constant during the scanning. When B_T is larger than 2.5 T, the total thermal ion heating effect becomes saturated (FIG. 3(b1)). However, the core plasma heating effect still changes. It is found that the best core plasma heating effect appears around B_T~2.56 T (FIG. 3(b2)). The resonance position in this case is about 6 cm at high field side from the axis. The absorption peak of ICRF power is at about ρ=0.17. The slight off-axis heating makes more power depositing in plasma core region (large plasma volume) rather than the exact on-axis heating (small plasma volume). Similarly, minority scanning is also performed. Based on the result of B_T scanning, B_T is set to 2.56 T in this scanning. Minority concentration varies from 1% to 7%. The optimized minority concentration may be 4%, for good ion heating effect and fair electron heating effect. Plasma density scanning from 1.5 to 3.0×10^{19} m^{-3} (line-averaged density) is then tested using B_T=2.56 T and n_{min}/n_e=4%. It is found that high density is good for global ion heating in this ICRF regime (FIG. 4(a1)) and density has strong influence on ICRF power deposition profile (FIG. 4(a2), ICRF power deposited in plasma core region varies.). The possible reason may be that

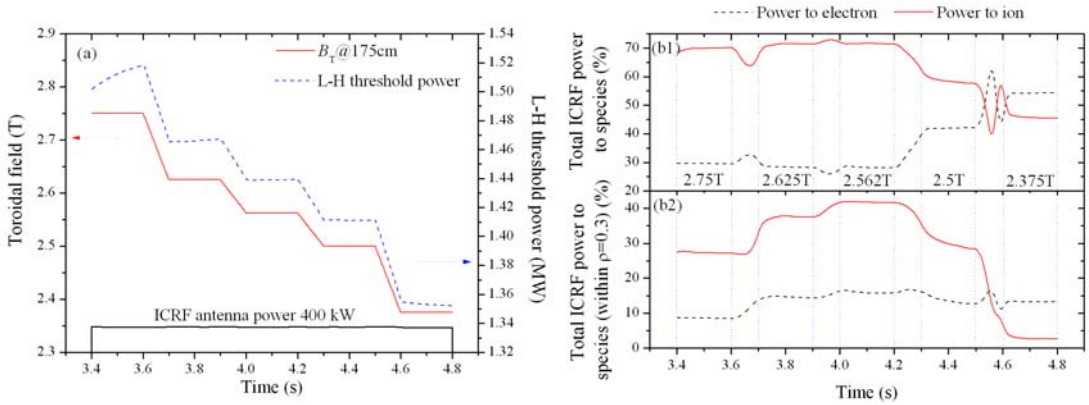

FIG. 3. Results of B_T scanning in ICRF ^{3}He minority heating plasma. The line-averaged density is 2.0×10^{19}m^{-3}. Minority concentration is 3%. (a) The waveform of ICRF power, B_T and its related L-H transition threshold power. (b) ICRF power deposited on bulk plasma species, after fast ion thermalization. (b1) shows the global effect, while (b2) shows the core region.

in low density (FIG. 4(b)), minority particles can reach very high temperature, e.g. 10 keV or higher in center when accelerating by E field in this case. This temperature mentioned here is the equilibrium temperature, for TORIC code treats any fast ions as a special ion species with an equivalent Maxwellian distribution. Thus, the Doppler effect of resonance is strong comparing with high density cases, making ICRF power strongly absorbed near plasma core. When density becomes higher (FIG. 4(c)), the Doppler effect is quite small because of lower minority temperature. A part of minority particles gains energy along Z direction at resonance position rather than in plasma core, causing the outward shift of absorption peak. If density is even higher (FIG. 4(d)), the degradation of Doppler effect becomes saturated. Meanwhile, absorption efficiency of single pass increases as density increases. More power is absorbed when wave is injected into plasma core region. The region of power absorption is not that scattered along Z direction comparing with FIG. 4(c), which causes the result of inward shift of absorption peak in power deposition profile. It is found that mode conversion also plays a role in the power deposition, especially at the case of 2.5×10^{19} m^{-3}.

4. High power EAST simulation

With the knowledge of ICRF simulation, high power EAST simulation is then performed using the parameters in Table I. The last column in Table I shows the different ICRH regimes and their frequencies used in different scenarios. In this set of simulations, the ^{3}He minority concentration (n_{min}/n_e) is set to 4%, which is the optimized value determined in section 3, and the concentration of hydrogen (n_H/n_e) in deuterium plasma is 20% as mentioned in plasma modeling in section 2. The highest stored energy in plasma that can be possibly achieved in current parameters is about 155 kJ. The temperature profiles of this run are shown in FIG. 5. The pedestal height is 440 eV for both electron and ion temperature profiles, and the pedestal locates at about ρ=0.92. Some related parameters are line-averaged density 3.0×10^{19} m^{-3}, based on the H mode profile in FIG. 1, effective total heating power P_{heat}=1.9 MW, including lower hybrid wave power P_{LHW}=300 kW, ICRF power P_{ICRF}=1.4 MW. Ohmic heating also contributes approximately 200 kW to the total heating power. Further, τ_E=74 ms, H_{98}=1.05, β_N=0.66. After calculating the volt-second consumption and the initial volt-second provided by TSC code, the possible discharge length of high power plasma in this set of simulations will be 8-200 s, depending on different scenarios of RF power combinations. Note that in this

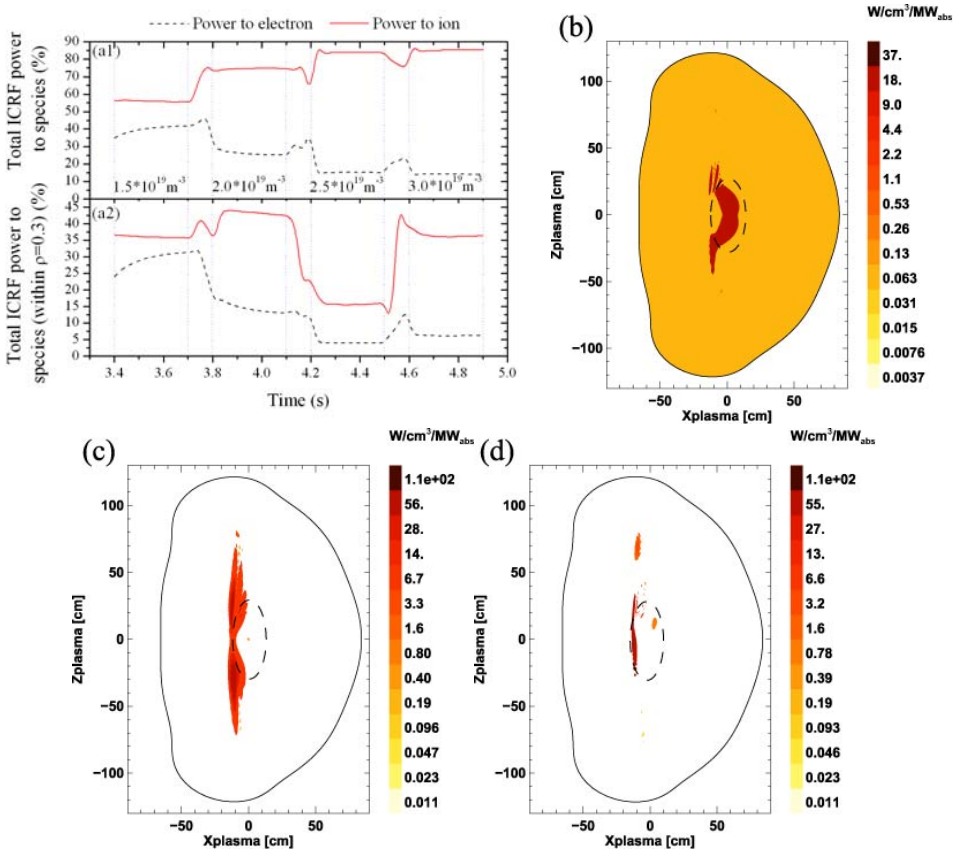

FIG. 4. Results of plasma density scanning. Base on previous scanning, B_T=2.56 T and n_{min}/n_e=4%. (a) ICRF power deposited on different thermal plasma species. (a1) global power deposition. (a2) power deposition in plasma core region ($\rho \leq 0.3$). (b)-(d) 2D diagrams of ICRF power deposition on ^{3}He (minority) with different line-averaged density. The dash line indicates the contour corresponding to ρ=0.3. (b) $2.0\times10^{19}m^{-3}$, (c) $2.5\times10^{19}m^{-3}$, (d) $3.0\times10^{19}m^{-3}$.

set of simulations, the total auxiliary heating power is selected to be several levels, which are shown in Table I. In each power level, different combinations of RF power (different ratio between ICRF and lower hybrid power) are tested. In the following part of this section, plasma features due to the RF power variation are introduced. Total heating power is generally considered as a critical factor that affects plasma feature, while there is not much discussion about the effect of different RF power combination on plasma feature. Thus, some results in this section are discussed in term of the ratio of ICRF or LHW power to total heating power. The different effect between ICRF and lower hybrid power on plasma features is therefore shown, in the cases of similar total heating power is held.

4.1 ICRF power deposition on thermal ions

The combination of RF power has influence on ICRF power deposition (minority heating regime) on thermal plasma species (FIG. 6), although plasma density and boundary condition (L or H mode) are the major factors. The influence of density is clearly identified in FIG. 4(a). This effect can also be seen in FIG. 6. Besides, fraction of ICRF power on thermal ions can be quite different (20% in high density and 40% in low density) between L and H modes even at the same line-averaged density. The influence of RF power combination is not that strong in comparison with density and boundary condition. The difference shown in FIG. 6 is about 5-15%. In ^{3}He minority heating regime, ICRF power does not deposit on thermal ions

TABLE I: PARAMETERS USED IN HIGH POWER EAST SIMULATION

Scenario	I_p (kA)	B_T (T)	$\bar{n}_e(10^{19}$ m$^{-3})$	P_{aux} (MW)	P_{L-H} (MW)	ICRH regime/ f (MHz)
L mode	500	2, 2.56	1.5∼3	0.6	–	SH/58, MH/25
H mode	500	1.8, 2	1.5, 2	0.9, 1.2	0.9∼1.18	SH/58
H mode	500	2.56	1.5∼3	1.7	1.22∼1.8	MH/25

directly. Minority species get the power first, and then transfer power to thermal ions via thermalization. Detailed analysis shows that more ICRF power (about 10% of its total power in high density case and 20% in low density case) can be deposited on minority species in L mode than that in H mode plasma. RF power combination has no effect in this phase. Besides, in the process of fast ion thermalization, minority species can transfer more power (as much as 20% of minority species power in high density case and 40% in low density case) to thermal ions in L mode plasma than that in H mode plasma. Varying RF power combination shows difference about 10-25% in this phase. It is clear that the major change of deposited ICRF power fraction on thermal ions is in the process of fast ion thermalization. In this simulation, one major difference between L and H mode boundary conditions can be considered as the change of density profiles. L mode has higher central plasma density than that of H mode if the line-averaged density is the same (FIG. 1). Meanwhile, the peak of absorbed ICRF power density is close to plasma center. Another major difference is H mode simulation has higher total heating power level (1.8 MW) than that of L mode (0.9 MW). In the process of fast ion thermalization, similar to NBI case, the electron heating fraction by minority particles is proportional to minority energy. High ICRF power increases minority energy. Low density also increases minority energy, which can be obtained from TORIC output. These two conditions all increase electron heating fraction by minority particles, while decreasing the final ICRF power deposited on thermal ions. Therefore, the reasons of difference due to density and RF power combination are straightforward. The difference of L and H mode conditions maybe partially because of the different power levels, and is partially because of the different central density.

4.2 Thermal diffusivity

χs also have relation with ICRF power, especially the χs in plasma core region. In FIG. 7(a), it is clear that ICRF power significantly enhances electron thermal diffusivity in plasma core region. Similar phenomenon is observed in ion channel. As mentioned in previous section, in this simulation, ICRH focuses on optimized ion heating effect, as well as plasma core heating effect. Higher fraction of ICRF power indicates higher power is injected in plasma core region (FIG. 7(b1)), because in this simulation, LHW power is usually deposited in the region of $0.4 \leq \rho \leq 0.6$. In FIG. 7(b1), total heating power deposited in plasma core region ($\rho \leq 0.3$) increases almost linearly as the fraction of ICRF power increases. Meanwhile, turbulence is excited. There is no available EAST model in nonlinear gyrokinetic code, such as GYRO or GS2. The growth rate of leading mode calculated by GLF23 is therefore shown in FIG. 7(b2) to provide the basic insight of the influence of heating power on turbulent instability. In this figure, growth rate at ρ=0.3 increases when the fraction of ICRF power increases, i.e. the heating power deposited in plasma core region increases. The trends for low and high total heating power cases are similar. No distinct difference can be observed. Due to the absence of rotation, no E×B shear stabilization is working to suppress the growing turbulence. The

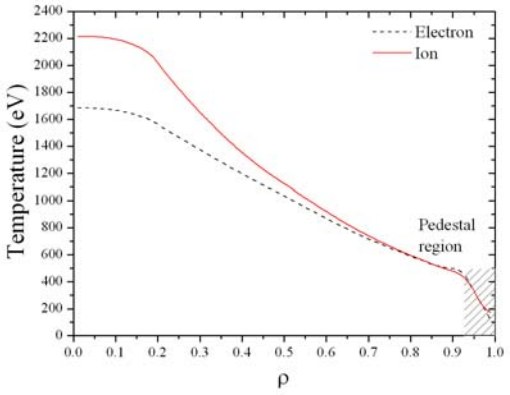

FIG. 5. Temperature profiles of the plasma with the highest stored energy.

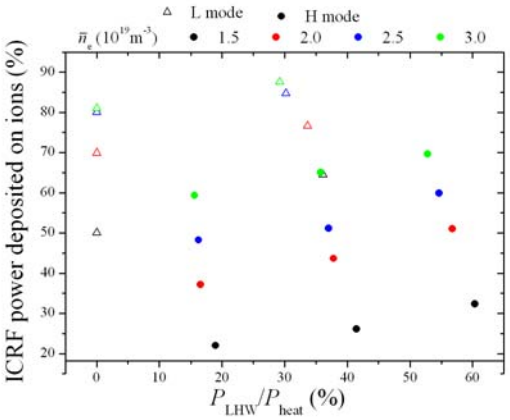

FIG. 6. Fraction of lower hybrid power has influence on ICRF power deposition on plasma species. Circle dots show H mode data, while triangular dots indicate L mode data. Data in different plasma density are shown in different colors.

anomalous thermal diffusivity is mainly determined by the growth rate of leading mode calculated by GLF23. The frequencies of leading mode usually are in the range of 200-450 kHz. They are in the typical temporal scale of ITG and dissipative TEM. Thus, ITG and/or (D)TEM may be responsible for the rise of thermal diffusivity when heating power increases. Regarding χs in outer radius, e.g. ρ=0.65, such a monotone increasing trend is very weak, because the power injected into this volume does not change much if total auxiliary heating power is fixed.

5. Conclusion

In this article, PTRANSP in combination with TSC has firstly applied on EAST simulation. After benchmarking against experiment data, GLF23 model is found to fit experiment data best and is selected for the further simulation. A set of parameter scanning simulation is performed for ICRH, which is new for EAST experiment. The optimized parameters are obtained in currently used plasma equilibrium and configuration and are further used in high power EAST simulation, which uses real EAST parameters for scenario development. Doppler effect and single pass efficiency are major factors that affect the power deposition. The different ICRF power deposition results in density scanning are also briefly discussed. In this set of high power EAST simulation, the possibly achieved highest plasma parameters are shown. Due to their different deposition positions, different RF power combinations may affect many aspects of plasma features, including ICRF power deposition fraction on thermal ions and thermal diffusivity. Thermal diffusivity in plasma core region can be largely enhanced (several times) by ITG and/or TEM turbulence excited by local power deposition. These phenomena will be further compared with experiment to validate PTRANSP code itself and its theoretical transport models. In order to do this, the TRANSP analysis of actual, well diagnosed, future high power experiments will be needed. The scenario development provides the capability of current EAST machine. And it is hoped that this kind of prediction work can help physicists learn the plasma feature in advance, and then design their proposals accordingly in the future.

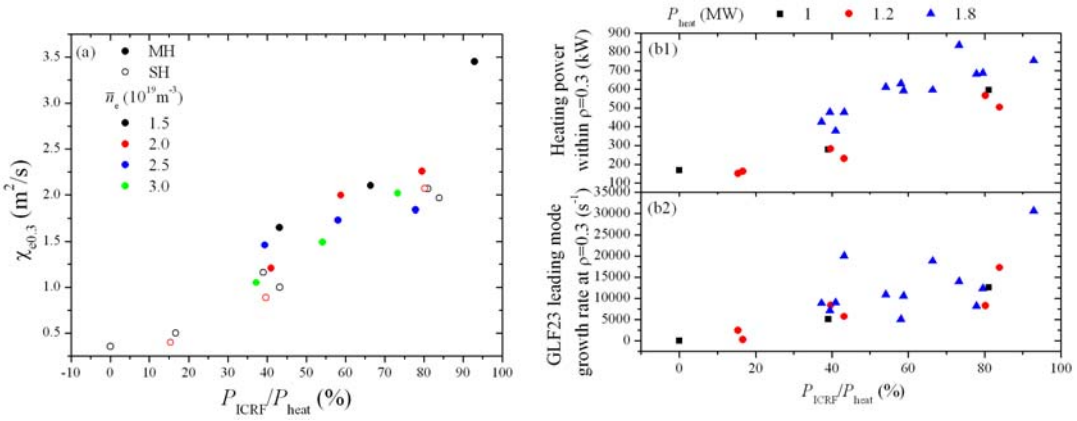

FIG. 7. (a) χ_e at ρ=0.3 vs fraction of ICRF power. Solid dots are ^{3}He minority heating data, and open dots are H second harmonic heating data. Different colors indicate different plasma density. (b) Heating power deposited in plasma core region and GLF23 leading mode growth rate vs ICRF power fraction. Data with three total heating power levels are involved. The square one is for 1 MW. The circle and triangle ones are for 1.2 and 1.8 MW, respectively.

Acknowledgments

The author S. Ding would like to thank TRANSP group at PPPL for their technical support during this study. This work is supported by the National Natural Science Foundation of China under Grant Nos. 10725523, 10721505, and 10605028

Reference

[1] Wan, B., et al., "Recent experiments in the EAST and HT-7 superconducting tokamaks", Nucl. Fusion **49** (2009) 104011.
[2] Budny, R.V., et al., "Predictions of H-mode performance in ITER", Nucl. Fusion **48** (2008) 075005.
[3] Goldston, R.J., et al., "New techniques for calculating heat and particle source rates due to neutral beam injection in axisymmetric tokamaks", J. Comput. Phys. **43** (1981) 61.
[4] Jardin, S.C., et al., "Dynamic modeling of transport and positional control of tokamaks", J. Comput. Phys. **66** (1986) 481.
[5] Doyle, E.J., et al., "Chapter 2: Plasma confinement and transport", Nucl. Fusion **47** (2007) S18.
[6] Kinsey, J.E., et al., "Transport modelling and gyrokinetic analysis of advanced high performance discharges", Nucl. Fusion **45** (2005) 450.
[7] Waltz, R.E., et al., "A gyro-Landau-fluid transport model", Phys. Plasmas **4** (1997) 2482.
[8] Bateman, G., et al., "Predicting temperature and density profiles in tokamaks", Phys. Plasmas **5** (1998) 1793.
[9] Kritz, A.H., et al., "PTRANSP Predictive Integrated Tokamak Modeling", 2009 EPS (Sofia)
[10] Bateman, G., et al., "Integrated predictive modelling simulations of burning plasma experiment designs", Plasma Phys. Control. Fusion **45** (2003) 1939.
[11] Brambilla, M., "Numerical simulation of ion cyclotron waves in tokamak plasmas", Plasma Phys. Control. Fusion **41** (1999) 1.
[12] Ignat, D.W., et al., "Dynamic modeling of lower hybrid current dirve", Nucl. Fusion **34** (1994) 837